The decisive role of hybridized electronic states on the appearance of superconductivity in Ba1-xKxMO3 (X=Bi, Sb)

Julien Varignon

The decisive role of hybridized electronic states on the appearance of superconductivity in $Ba_{1-x}K_xMO_3$ (X=Bi, Sb)

Julien Varignon[1]

[1]Laboratoire CRISMAT, CNRS UMR 6508, ENSICAEN, Normandie Université,

6 boulevard Maréchal Juin, F-14050 Caen Cedex 4, France

Abstract

The observation of superconductivity in hole doped antimonates $Ba_{1-x}K_xSbO_3$ (BKSO), isoelectronic compounds to bismuthates $Ba_{1-x}K_xBiO_3$ (BKBO) superconductors, enables a pathway to clarify the role of hybridizations between electronic states of metals and ligands on the emergence of superconductivity. Herein, using *first-principles* simulations, the localized electronic structure of antimonates is demonstrated to produce various charge and bond orderings (CBO) up to x=0.6, hence hindering the appearance of a superconducting state. This is in contrast with bismuthates where the formation of charge orderings is suppressed by doping effects and their native hybridized electronic structure. Although quenched by doping effects, the CBO mediate the Cooper pairs formation and the resulting electron-phonon coupling reproduces the experimental facts such as a larger T_c in BKSO than in BKBO for x>0.65 and a maximal T_c of ~30K observed at x=0.4-0.5 for BKBO. The latter point is ascribed to a soft phonon mode at x=0.5 while the former observation is ascribed to an intrinsically stronger coupling between lattice distortions and electrons in $BaSbO_3$. Although materials with a localized electronic structure could warrant larger T_c's, the main drawback is the resilience of such compounds to form a metallic state and hence superconductivity emerges far away of soft phonons possessing a strong coupling with the electronic structure.

I. Introduction

Superconductivity (SC) is certainly one of the most fascinating property of materials characterized by zero electrical resistance to direct current and perfect diamagnetism. It is explained on the basis of bound electrons forming Cooper pairs [1]. In the Bardeen, Cooper and Schrieffer (BCS) theory [2], the formation of Cooper pairs is explained by exchange of phonons. In many other systems, proximity of a charge ordered (CO) state or a magnetic phase transition is proposed to be a key behind the formation of bound electrons. Strong correlation effects that have to be accounted in electronic structure simulations [3–11] and/or strong hybridizations between metals and anionic *p* states [12–15] are also proposed to be a determining factor behind superconductivity.

One can usually quantify the level of hybridization between the metal and the anionic O states by evaluating the charge transfer energy ΔE_{CT} that is the energy difference between the center of the bands associated with relevant metallic (E_m) and oxygen (E_o) levels (*i.e.* $\Delta E_{CT}=E_m-E_o$). A negative (positive) ΔE_{CT} then corresponds to strongly (weakly) hybridized and hence delocalized (localized) electronic structures. These two types of regime are therefore coined as negative and positive charge transfer (NCT and PCT) regimes, respectively. Emblematic examples of materials falling within the NCT regime are the cuprates or the bismuthates that are both superconductors once appropriately doped with electrons and/or holes [3,12,16–18]. However, the lack of isoelectronic superconductors long hindered the exploration of the precise role of hybridizations between metals and anion states on the emergence of SC in oxides. The discovery of SC in hole doped $BaSbO_3$ (BSO), an isoelectronic material to bismuthates $Ba_{1-x}K_xBiO_3$ but that belongs to the PCT regime, thus offers an ideal testbed for clarifying the role of hybridizations [19].

In bulk, BSO adopts a slightly distorted ABO_3 perovskite structure characterized by a bond disproportionation B_{oc} mode producing a rock salt pattern of compressed O_6 groups and extended octahedra (**Figure 1.a).** It originates from an unstable 4+ formal oxidation state (FOS) of Sb cations ($5s^1$ electronic configuration*)* that prefers to disproportionate to the more stable 3+ ($5s^2$) and 5+ ($5s^0$) FOS in the ground state [20], yielding a CO insulating state with Sb cations sitting in an extended (Sb^{3+}) and compressed (Sb^{5+}) octahedra. Once sufficiently doped with holes by forming a $Ba_{1-x}K_xSbO_3$ solid solution ($0.65<x<0.8$), the material becomes a superconductor with a critical temperature T_c up to 15 K for $x=0.65$ [19].

At first glance, the observation of superconductivity in hole doped BSO is expected since it is isostructural and isoelectronic to bismuthates ($BaBiO_3$ and $SrBiO_3$) that both exhibit SC once

appropriately hole-doped [16,18,21,22]. Nevertheless, these two family of compounds show noticeable differences: (i) the doping content needed to transit from a charge and bond ordered (CBO) insulating state to the superconducting region is smaller in $Ba_{1-x}K_xBiO_3$ (BKBO, x~0.4) than in $Ba_{1-x}K_xSbO_3$ (BKSO, x>0.6); (ii) BSO falls within the PCT regime with ΔE_{CT}= 0.76 eV while $BaBiO_3$ is in a NCT regime with ΔE_{CT}= -2.45 eV [19]; (iii) T_c reaches 32 K in BKBO around x=0.4-0.5 [18,21] while it does not exceed 15 K in the optimally doped BKSO [19] and (iv) BKSO exhibits larger T_c's than BKBO for x>0.65. Although a triggered mechanism between octahedral rotations and the disproportionation effects could promote a strong stability of the B_{oc} mode [23,24], this possibility is ruled out by an apparent absence of octahedral rotations in antimonates. One may thus ask: (i) "*possessing the same roots in the undoped starting phase, is superconductivity also reached at the proximity of a CBO state in BKSO as in BKBO (and $Sr_{1-x}K_xBiO_3$)?*"; (ii) "*what is the intrinsic difference responsible for the largest doping content needed to reach the superconducting region in BKSO than in BKBO?*"; *(iii)* "*what are the determining factors behind the larger T_c exhibited by BKSO than BKBO for x>0.65 and (iv) why is the maximal T_c of BKBO larger than that of optimally doped BKSO*?"

In this article, using Density Functional Theory (DFT) involving all relevant degrees of freedom and a parameter free meta-GGA revised Strongly Constrained and Appropriately Normalized (R2SCAN) [25] functional, antimonates are identified to possess a stronger electronic instability towards charge and bond disproportionation effects associated with the unstable 4+ FOS of B site cations than bismuthates. This strong tendency to form CBO is resilient to hole doping BKSO for x=0 to x=0.6, thereby hindering the apparition of a metallic phase. This is ascribed to the ionic nature of the electronic structure of antimonates that favors a localized states. In contrast, the NCT nature and the resulting delocalized electronic structure of bismuthates already screen the tendency toward disproportionation, thereby requiring a lower doping content to transit to a metallic phase. Once doping totally quenches the formation of the various CBOs, the electron-phonon couplings (EPC) associated with the CBO remain sufficiently large to mediate the formation of Cooper pairs. Nevertheless, the EPCs for x>0.65 are larger in BKSO than in BKBO due to a stronger coupling between structural displacements and the electronic structure, resulting in larger T_c's for BKSO than for BKBO at a fixed doping content. Finally, the maximal T_c reached at x=0.5 in BKBO originates from a CBO phonon mode that reaches a low frequency at x=0.5, thereby producing a maximal EPC. Thus, although materials with a localized electronic structure possess a strong coupling between structural distortions and electrons, the drawback of such compounds is their resilience to doping effects thereby hindering the emergence of a superconducting phase close to soft phonon modes.

II. Methods

1) DFT simulations

DFT calculations are performed with the Vienna Ab initio Simulation Package (VASP) [26,27]. In order to appropriately amend the self-interaction errors inherent to practiced DFT, the meta-GGA revised Strongly Constrained and Appropriately Normalized (R2SCAN) [25] functional is employed. This type of meta-GGA functional was previously shown to be accurate in capturing the correct trend of insulating to superconducting transition as a function of doping content in isoelectronic and isostructural bismuthates [24]. It further allows a parameter free calculation with a functional able to adapt to different formal oxidation states (FOS) showed by a single ion. The energy cut off is set to 650 eV and atomic positions plus lattice parameters are optimized until forces acting on each atom are lower than 0.005 eV/Å. Projector Augmented Waves (PAW) [28] potentials are used for modelling core electrons with the following VASP 5.4 Perdew Burke Ernzerhof (PBE) POTCAR files: Ba_sv, K_sv, Sb, Bi and O. The cation substitutions are extracted by using the special quasi random structure (SQS) allowing to identify the cation arrangement maximizing the disorder characteristic of a solid solution [29]. This was successfully applied to capture trends in insulator to metal transition through doping effects in $Sr_{1-x}K_xBiO_3$ [24] or in $Sm_{1-x}Ca_xNiO_3$ solid solutions [30]. The atomic positions are provided in **Tables SI1** and **SI2** in the **supplementary material 1** [31]**.** Solid solutions are modelled by using a 32 f.u corresponding to a $(2\sqrt{2}, 2\sqrt{2}, 4)$ supercell, or a 27 fu with a (3, 3, 3) supercell, with respect to the high symmetry primitive *Pm-3m* cell exhibited by perovskite materials. Several structural starting points are considered for each doping content, corresponding to potential lattice distortions able to localize electrons. For instance, a charge ordered $Ba_{2/3}K_{1/3}SbO_3$ should correspond to a material with 1 Sb^{3+} and 2 Sb^{5+}, it should then induce a distortion with a $\vec{q}$ vector of either (1/3, 0, 0), (1/3, 1/3, 0) or (1/3, 1/3, 1/3). In order to reduce the computational effort, preliminary checks are performed on smaller unit cells compatible with a given distortion mode and doping content. Then, these cells are transformed into larger supercells in order to have a better representation of the solid solution with 32 or 27 fu.

2) Superconducting quantities:

Using the methodology presented in Ref. [32], the electron-phonon coupling constant λ is computed as:

$$\lambda = \frac{2N(E_F)}{N_{\vec{q}}} \sum_{\vec{q},\nu} \frac{\hbar^2}{2M_X \omega_{\vec{q},\nu}^2} \left| D_{\vec{q}}^{\nu} \right|^2 \quad \textbf{(equation 1)}$$

where $N(E_F)$ is the density of states at the Fermi level E_F, $N_{\vec{q}}$ is the number of $\vec{q}$ points considered, M_X is the mass of moving atoms, $\omega_{\vec{q},\nu}$ is the frequency of the mode ν at the point $\vec{q}$ and $\left| D_{\vec{q}}^{\nu} \right|$ is the

"Reduced Electron-Phonon Matrix Element" (REPME). The latter quantity is extracted by estimating the band splitting ΔE_b induced by the addition of the eigen displacement of the $(\vec{q}, \nu)$ phonon mode in the ground state with the amplitude $u_{\vec{q},\nu}$ per moving atom:

$$D_{\vec{q}}^{\nu} = \left|\frac{\Delta E_b}{2u_{\vec{q},\nu}}\right| \quad \textbf{(equation 2)}$$

The frequency $\omega_{\vec{q},\nu}$ of the mode ν at the point $\vec{q}$ is obtained by fitting the total energy E versus mode amplitude $Q_{\vec{q},\nu}$ of a $(\vec{q},\nu)$ phonon starting from the ground state structure with a polynomial expression of the form $E(Q_{\vec{q},\nu}) = aQ_{\vec{q},\nu}^2 + bQ_{\vec{q},\nu}^4$. Recalling that the energy of an harmonic oscillator is given by $\frac{1}{2}M_X\omega_{\vec{q},\nu}^2 Q_{\vec{q},\nu}^2$, the frequency $\omega_{\vec{q},\nu}$ is

$$\omega_{\vec{q},\nu} = \sqrt{2a/M_X} \quad \textbf{(equation 3)}$$

The critical temperature T_c of the material is computed using the Mc Millan-Allen equation [33]

$$T_c = \frac{\hbar\omega_{log}}{1.2}\exp\left(-\frac{1.04\lambda}{\lambda-\mu^*(1+0.62\lambda)}\right) \quad \textbf{(equation 4)}$$

where μ* is the screened Coulomb potential with typical values between 0.1 and 0.15 and ω_{log} is the logarithmic frequency estimated as

$$\omega_{log} = \left(\prod_i^n \omega_i\right)^{1/n} \quad \textbf{(equation 5)}$$

3) Wannier functions

In order to extract localized atomic-like functions, Wannier functions (WF) are built from the DFT band structure. To that end, the 10 Kohn-Sham states located around the Fermi level for a primitive cubic cell are projected on initial guess functions of B-*s* (1 state) and O-*p* (9 states) characters in order to get the initial gauge for the localization procedure [34–36]. The density of states can then be built on the basis of these localized atomic-like functions. Using the onsite energies associated with the WFs, the charge transfer energy is computed as the energy difference $\Delta E_{CT}=E_s-E_p$.

4) Other details

Band structures are unfolded to the primitive high symmetry *Pm-3m* cell of perovskites using the VaspBandUnfold code [37]. Symmetry of relaxed structures are obtained using FINDSYM [38] and amplitudes of distortions with respect to a primitive high symmetry *Pm-3m* cell are extracted using amplimodes of the Bilbao crystallographic server [39] and the isotropy suit of softwares [40].

III. Results and Discussion

1) Electronic structure of bulk $BaSbO_3$

Electronic and structural properties of pristine $BaSbO_3$ are first studied. After the structural relaxation of the bulk material, $BaSbO_3$ is identified to adopt a *R-3* structure at 0 K characterized by an $a^-a^-a^-$ anti-phase octahedral rotation in Glazer's notation as well as a bond disproportionation B_{oc} mode. From a symmetry mode analysis with respect to primitive high symmetry *Pm-3m* cell adopted by perovskites, the octahedral rotation (labelled Ø) and B_{oc} distortion exhibit sizeable amplitude of distortions with $Q_{Ø}$=0.130 Å/f.u and Q_{Boc}=0.191 Å/f.u, respectively. The amplitude of B_{oc} is in sharp agreement with the experimental value of Q_{Boc}=0.187 Å/f.u extracted from the structure at 300K from Ref. [19]. It is worth to emphasize that no octahedral rotations have been identified at 300K but they likely appear at lower temperature. The energy lowering event associated with the O_6 rotations with respect to a cell with only the B_{oc} mode is indeed extremely small (ΔE=-0.7 meV/f.u). This is also suggested by an imaginary frequency of the Ø mode from the *first-principles* calculations on $BaSbO_3$ presented in Ref. [41].

The effect of the B_{oc} mode is to split the Sb cations into two different cations (**Figure 1.a**): a Sb cation sits in an extended octahedra (labelled Sb_L) while all its first nearest neighbor Sb cations are located in a compressed O_6 group (labelled Sb_S). It hence produces a clear asymmetry of the electronic structure between the two types of Sb cations and open a band gap of 0.90 eV as shown by the projected density of states reported in **Figure 1.b**. One further notices that Sb_L cations are fully occupied, in contrast to Sb_S cations that show partly unoccupied *s* states, compatible with disproportionation effects. Finally, one observes that unoccupied states are predominantly formed by the B cation states rather than O-*p* states, hindering at the fact that this compound is characterized by a localized electronic structure rather that by Bi-*s* and O-*p* hybridized states as in $BaBiO_3$ – see **supplementary material 2**.

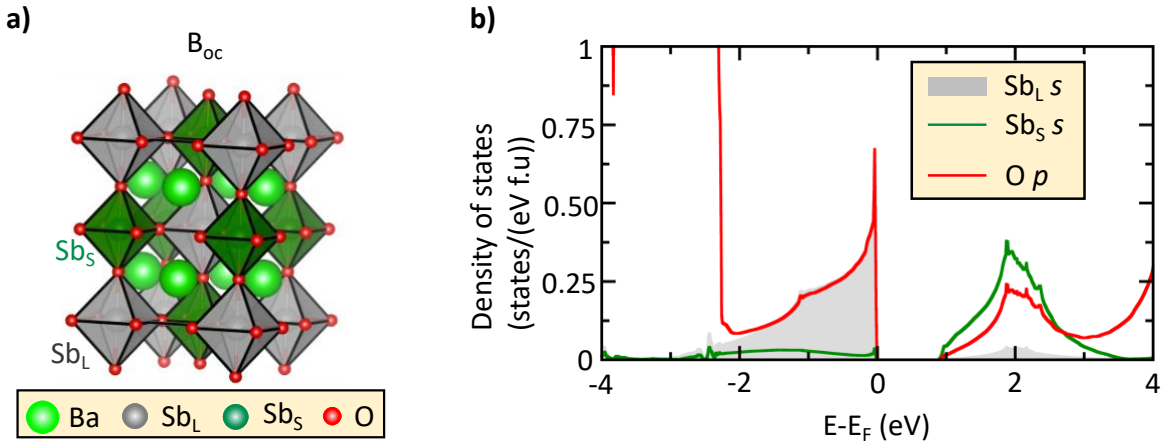

Figure 1: Structural and electronic properties of $BaSbO_3$. a) *Breathing (B_{oc}) structural distortion exhibited by $BaSbO_3$ and producing different O_6 groups around Sb cations.* ***b)*** *Projected density of states*

on Sb_L (filled grey area) and Sb_S (green line) s states and O-p states (red line) around the Fermi level in the R-3 ground state.

2) The doped phase diagram

Figure 2 displays the phase diagram of BKSO solid solutions as a function of *x*. At low doping content x=0.125, two bipolaronic states are stabilized in the material with holes created on Sb_L cations that are doubly occupied in the pristine material. This is accompanied by the collapsing of the local O_6 octahedra due to the increase of the FOS of the local Sb cations. The average B_{oc} mode amplitude decreases to Q_{Boc}=0.161 Å/f.u for x=0.125, albeit it is sufficient to produce a semiconducting state with a band gap of 0.74 eV. Further increasing the doping content transforms the system into a metal at x=0.25, yet with a persistent breathing mode B_{oc}. The latter only vanishes at x=0.4375.

Although one would expect a metallic non-CBO phase above x=0.25, alternative bond disproportionation distortions, labelled alt-$B_{oc1/3}$ and alt-$B_{oc1/2}$ and sketched in **Figure 2**, emerge for x=1/3 and x=0.50. These lattice distortions are associated with peculiar CO producing large octahedra and compressed O_6 groups accommodating a given charge orderings. These modes reach their maximum at x=0.5 and x=1/3, which corresponds to $Ba_{0.5}K_{0.5}SbO_3$ and $Ba_{0.66}K_{0.33}SbO_3$ solutions, respectively. At x=0.5 (x=1/3), Sb cations are in a nominally 4.5+ (4.33+) FOS but in fact they prefer to disproportionate into $4Sb^{4.5+} \rightarrow 3Sb^{5+} + Sb^{3+}$ ($3Sb^{4.33+} \rightarrow 2Sb^{5+} + Sb^{3+}$) in the ground state. Above x=0.5, all solutions are found metallic without the presence of B_{oc} and alt-B_{oc}'s modes. Hence, all types of CO vanish for x>0.5625.

The existence of multiple CBO is compatible with experiments showing two distinct CBO in the doped phase diagram of antimonates up to x>0.5625 [42]. Notably, a distortion pattern compatible with 1 large O_6 group (Sb^{3+}) surrounded by 3 smaller octahedra (Sb^{5+}) at x=0.5 is reported experimentally although the symmetry is different from the DFT result -- *I_4/mmm* space group with the present DFT *vs I_4/mcm* in Ref.[[20]]. This slight discrepancy may originate from the limited supercell size used in the simulations. The existence of a bond disproportionation appearing at the M point ($\vec{q}$=(1/2,1/2,0)) is also suggested by DFT calculations of Ref. [41] with the existence of an imaginary frequency in the cubic cell of x=0.5 doped antimonates. Furthermore, the extinction of all CBO closely relates with the appearance of the superconducting region experimentally (x>0.6). It is worth to emphasize that the R2SCAN functional may slightly underestimate the band gaps and hence might shift the insulating-to metal-to superconducting transition as a function of *x* to slightly smaller doping contents than the experimentally observed content. The existence of multiple CBO in BKSO is surprising

since isoelectronic BKBO does not develop such a propensity toward the alt-B_{oc} modes for instance. Indeed, similar structural relaxations in BKBO only reveal a B_{oc} mode that is rapidly quenched upon doping (**Figure 2)**. One concludes here that the superconducting transition of antimonates (and bismuthates) is at the vicinity of a stable CO phase.

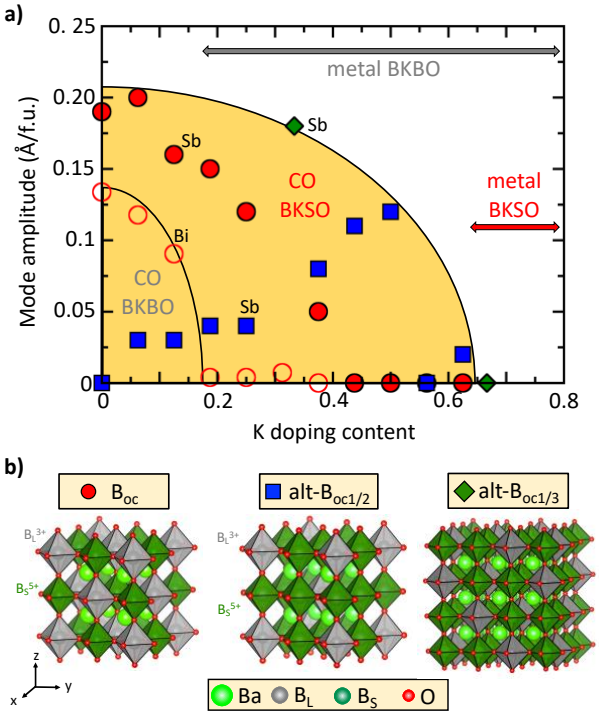

***Figure 2**: **Doped phase diagram of antimonates and bismuthates. a)** Evolution of the B_{oc} (red circles), alt-$B_{oc1/2}$ (blue squares) and alt-$B_{oc1/3}$ (green diamonds) mode amplitude (in Å/f.u) as a function of the doping content x in $Ba_{1-x}K_xSbO_3$ (filled symbols) compound and $Ba_{1-x}K_xBiO_3$ (unfilled symbols). **b)** Sketches of the three main bond disproportionation modes identified in doped antimonates. B_{oc}, alt-$B_{oc1/2}$ and alt-$B_{oc1/3}$ appear at the (1/2,1/2,1/2), (1/2,1/2,0) and (1/3,1/3,0) points of the Brillouin zone.*

3) Potential energy surfaces associated with disproportionation modes

In order to understand the different response to hole doping effects between BKBO and BKSO, potential energy surfaces (PES) associated with disproportionation distortions starting from a perfectly undistorted high symmetry *Pm-3m* cell are computed at x=0, x=0.33 and x=0.50 (**Figures 3.a-c**). At x=0, the B_{oc} mode PES is characterized by a double well potential whose minimum is located at non-zero amplitude for the two materials. It follows that the B_{oc} mode spontaneously appears in the compounds, signaling the presence of an instability toward disproportionation effects of the 4+ FOS of Sb and Bi cations. Nevertheless, the B_{oc} mode is associated with a large energy gain in $BaSbO_3$ (ΔE=-160 meV/f.u) while it is much smaller in $BaBiO_3$ (ΔE=-15 meV/f.u). Regarding the alt-$B_{oc1/2}$ and alt-$B_{oc1/3}$ modes at

x=0.5 and x=0.33, respectively, double well potentials with a minimum located at non-zero amplitude are identified in $BaSbO_3$ while $BaBiO_3$ does not have a propensity to develop these alternative disproportionation modes.

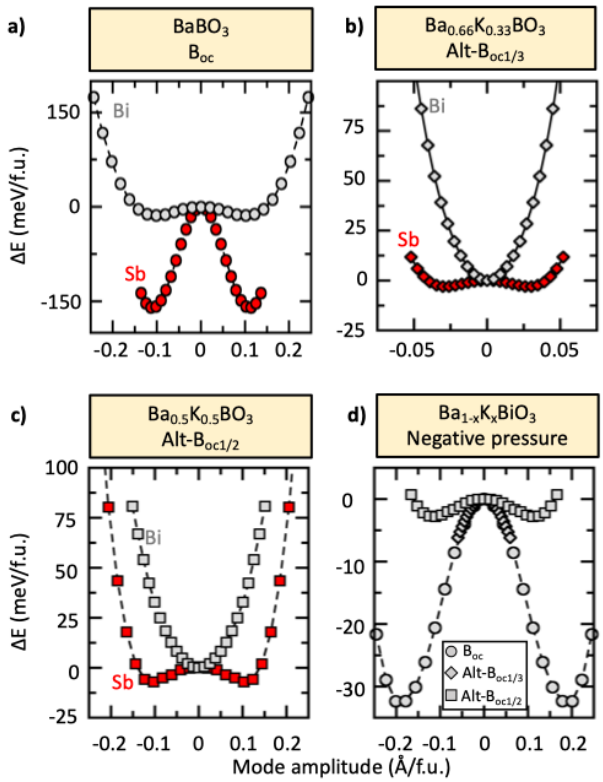

Figure 3: Potential energy surfaces associated with the B_{oc} and alt-B_{oc} structural distortions. *Energy gain ΔE (in meV/f.u) associated with the condensation of amplitudes (in Å/f.u) of either B_{oc} (circles), alt-$B_{oc1/3}$ (diamonds) or alt-$B_{oc1/2}$ (squares) in 0%, 33% and 50 % doped $BaSbO_3$ (in red) and $BaBiO_3$ (in grey) starting from a high symmetry cubic cell with a lattice parameter yielding the ground state volume of relaxed doped compounds. A negative pressure expanding the cubic cell parameter by 10% is also considered (**d**). The reference energy is taken at zero amplitude of the modes. Irreducible representation are R_2^-, M_1^+ and LD_1 for B_{oc}, alt-$B_{oc1/2}$ and alt-$B_{oc1/3}$ distortions, respectively, when the A site cation is considered at the corner of the cell.*

4) Localized (hybridized) electronic structures are at the core of the multiple (absence of) CBOs:

The tendency to develop instabilities toward disproportionation effects or Jahn-Teller effects is strongly dependent on the level of hybridization between relevant B cation and O *p* states as well as the compacity of bands in perovskites [43–46] – *i.e* compact states increase correlation effects while

hybridizations do screen them. In order to understand the different tendency in disproportionation effects between BKSO and BKBO, one can start from a cubic cell of the pristine compounds. By looking at the projected band structure on B-*s* and O-*p* states of **Figure 4.a**, one identifies that : (i) the bandwidth W of states undergoing disproportionation effects are more compact in BBO (W=5.12 eV) than in BSO (W=5.78 eV) and (ii) the band crossing the Fermi level is dominantly of B-*s* character in BSO while it is dominantly of O-*p* character in BBO. Point (ii) is further confirmed by projected density of states on B-*s* and O-*p* characters presented in **Figure 4.b**. By adjusting the lattice parameter of each compounds by +/- 5%, the bandwidth W as well as the hybridized character of states are driven by geometric effects (**Figures 4.b** and **5.a**) : W decreases with increasing the cell volume while the B cation character of bands crossing the Fermi level increases with decreasing the cell volume.

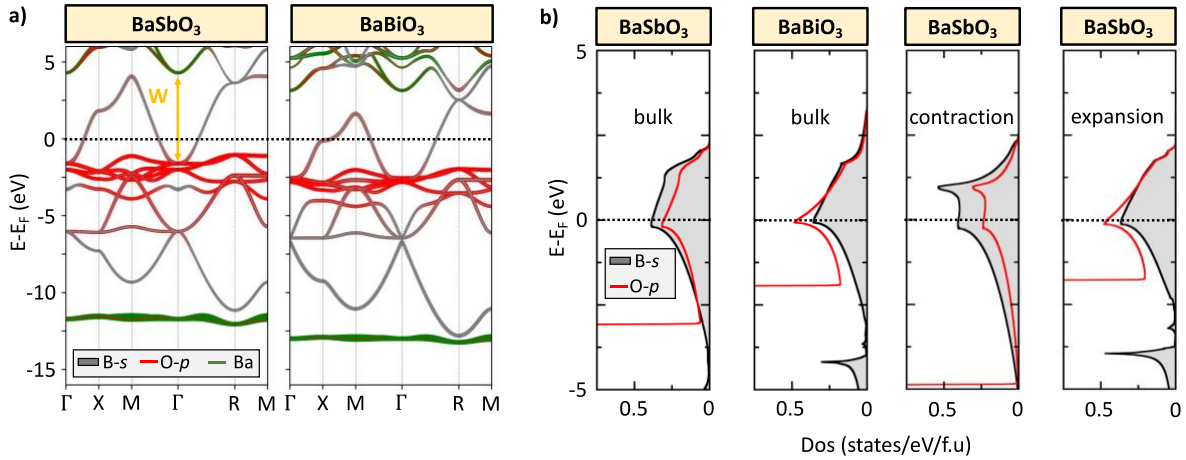

***Figure 4**: **Electronic properties of cubic cells**. **a)** Band structure within the cubic cell of $BaSbO_3$ and $BaBiO_3$ projected on B-s (grey), O-p states (red) and Ba (green) contributions. **b)** Projected density of states on B-s (grey) and O-p states (red) in $BaSbO_3$ and $BaBiO_3$ in bulk and in $BaSbO_3$ with a cell expansion/contraction of 5% of the cubic lattice parameter. The horizontal dashed line corresponds to the Fermi level. The high symmetry points are Γ (0,0,0), X (½, 0,0), M(½, ½,0) and R (½,½,½). The dos is plotted on the basis of Wannier functions.*

The role of W and hybridizations on the tendency toward disproportionation effects can be tracked by recomputing the potential energy surfaces of the B_{oc} mode for the two compounds but with lattice parameters expanded or contracted by 5%. The energy gain ΔE associated with the stabilization of the B_{oc} mode as well as the fractional amplitude Q_{Boc} of stabilized B_{oc} mode are reported on **Figure 5** (potential energy surfaces are available in **supplementary 3**). In both cases, the tendency toward disproportionation effect increases with increasing the cell volume, but energy gains are an order of magnitude larger in BSO than in BBO. The very same trend is observed for the stabilized amplitude Q_{Boc} of B_{oc} mode in the structure. The increased tendency toward disproportionation effect with increasing

the lattice parameter is explained by a reduced bandwidth in both compounds. Even though BBO and BSO would exhibit the same lattice parameter, ΔE in BBO would remain an order of magnitude smaller than in BSO. This is due to the fact that the O-*p* character of the states crossing the Fermi level ultimately increases and becomes dominant over B cations states (**Figure 4.b**) with increasing the cell volume, thereby screening the tendency toward disproportionation effects. Therefore, the larger tendency toward disproportionation effect of BSO with respect to BBO is explained by the intrinsically more ionic character of its electronic structure – and hence its more correlated nature.

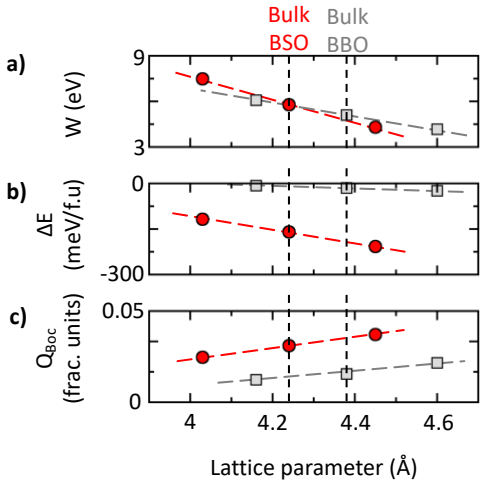

Figure 5: Trends of disproportionation effects as a function of the cubic cell lattice parameter*. Evolution of the bandwidth W (in eV, **a**), energy gain associated with the condensation of the B_{oc} mode (in meV/f.u., **b**) and fractional amplitude Q_{Boc} of stabilized B_{oc} mode (in fractional units, **c**) starting from a perfectly undistorted cell of compounds as a function of the lattice parameter in $BaSbO_3$ (in red) and $BaBiO_3$ (in grey). The normalized Q_{Boc} is obtained by dividing the amplitude of distortions by the cell parameter.*

The hybridized electronic structure of $BaBiO_3$ then explains the fact that the alt-$B_{oc1/2}$ and alt-$B_{oc1/3}$ are not stabilized in $Ba_{1-x}K_xBiO_3$ for x=1/2 and x=1/3, respectively. In order to confirm this result, the bandwidth W of relevant states undergoing the disproportionation effects is decreased to W=3.88 eV by applying a cell parameter expansion of 10% *vs* W=6.20 eV for the bulk phase. It then produces a slight double well potential for the alt-$B_{oc1/2}$ mode albeit its energy gain ($\Delta E_{alt\text{-}Boc1/2}$=-2.8 meV/f.u) remains smaller than that observed in unpressured antimonates ($\Delta E_{alt\text{-}Boc1/2}$=-7.1 meV/f.u). The observation of quenched disproportionation modes with hybridization and doping effects is in sharp agreement with experiments: BKSO becomes a SC for x>0.65 while BKBO is SC for x>0.35. One concludes here that doping as well as hybridized electronic structures are a knob quenching all CBOs.

5) Superconducting properties

Being able to produce an insulating state in the underdoped regime of BKSO and BKBO, and quenched by doping and hybridization effects, one may wonder if "*CBO lattice vibrations can produce a sufficiently large electron-phonon coupling (EPC) for explaining Cooper pairs formation and the superconducting temperature in the appropriately doped region*". **Figure 6** reports the main superconducting quantities of doped $BaSbO_3$ and $BaBiO_3$ necessary to compute the electron-phonon coupling with **eq.1** (band structures of doped compounds are presented in **supplementary material 4**). In $BaSbO_3$, the frequency of the different disproportionation modes increases with increasing the doping content in the SC region. Such a behavior is also observed in $BaBiO_3$ at the exception of the alt-$B_{oc1/2}$ mode that only increases for x>0.5 and is nearly constant with a minimum at x=0.5. This is explained by the fact that this mode is compatible with a half doped situation that would result in a charge ordering with $4Bi^{4.5+}$ transforming to $3Bi^{5+}$ + $1Bi^{3+}$, should the material be characterized by a localized electronic structure.

The Reduced Electron Phonon Matrix Elements (REPME), labelled D, increases with increasing the doping content for all disproportionation modes at the exception of the alt-$B_{oc1/2}$ mode that shows a constant value with x. One highlights that the REPMEs are globally larger in $BaSbO_3$ than in $BaBiO_3$, at the exception of the B_{oc} mode that has roughly the same magnitude in both compounds. This closely relates to the appearance of this mode in the pristine form of both materials. The larger REPMEs for alt-B_{oc} modes in $BaSbO_3$ is likely originating from the PCT nature, and hence more localized electronic structure, of antimonates inducing a stronger electron-electron interaction.

Regarding the squared density of states (dos) for several doped compounds, one observes a linear trend as a function of the doping content *x*. This is compatible with a free electron gas in which the density of states evolves as $\sqrt{(E - E_0)}$ – the doping content *x* is acting on the E-E_0 value where E_0 is the bottom of the parabola. Finally, it is worth to emphasize that the squared dos is larger in BKBO than in BKSO, compatible with the fact that the bandwidth is smaller in $BaBiO_3$ than in $BaSbO_3$.

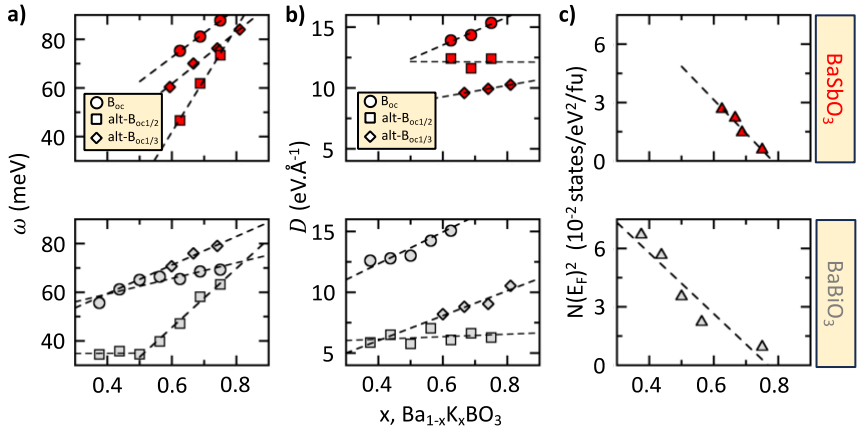

Figure 6: Superconducting quantities. *Frequency ω (in meV,* ***a****), reduced electron phonon matrix element D (in eV/Å,* ***b****) for the B_{oc} (circles), alt-$B_{oc1/2}$ (squares) and alt-$B_{oc1/3}$ (diamonds) modes and squared density of states at the Fermi level $N(E_F)$ (in states/eV²/f.u,* ***c****) in $BaSbO_3$ (red) and $BaBiO_3$ (grey). The dashed lines correspond to linear fits of the DFT results.*

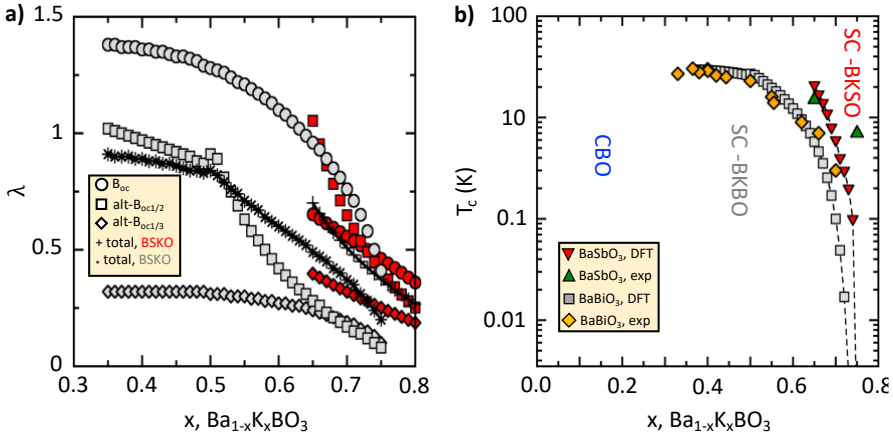

Figure 7: Superconducting properties of $Ba_{1-x}K_xSbO_3$ and $Ba_{1-x}K_xBiO_3$ compounds. *Computed electron-phonon coupling constant λ (****a****) associated with the B_{oc} (circles), alt-$B_{oc1/2}$ (squares) and alt-$B_{oc1/3}$ (diamonds) modes in BKSO (red) and BKBO (grey) and computed critical temperature T_c (in K,* ***b****) versus the doping content in $BaSbO_3$ (down red triangles) and $BaBiO_3$ (grey squares). A screened Coulomb potential μ*=0.125 is used. Experimental values for $BaBiO_3$ (orange diamonds) and $BaSbO_3$ (up green triangles) are extracted from Refs.* [19,47,48].

Figure 7.a displays the evolution of the EPC associated with each CBOs in BKSO and BKBO as a function of the doping content and obtained from fits of $N(E_F)$, D and ω as a function of the doping content (see **supplementary material 5**). All EPCs decrease with increasing the doping content, in agreement with the extinction of the tendency toward CBO identified at lower doping content. The optimally doped BKBO (x=0.4-0.5) presents a total EPC – computed as the average of the EPC induced

by the three disproportionation modes (**see eq.1**) around 1, in agreement with experimental values suggesting an EPC of 1.3 ± 0.2 [8] and previous theoretical works [9–11,24]. This EPC then rapidly decreases and becomes smaller than the total EPC of BKSO for x>0.6. This is in agreement with previous DFT calculations showing such a trend [10]. Finally, the alt-$B_{oc1/2}$ and alt-$B_{oc1/3}$ modes have a larger contribution to the total EPC in BKSO than in BKBO for x>0.65, thereby producing a larger total EPC in BKSO for these doping contents.

One can then estimate the critical temperature T_c using the modified Mac Millan equation presented in **eq.4** where ω_{log} is the logarithmic averaged phonon frequency (expressed in K) and μ^* is the screened Coulomb potential with conventional values usually ranging from 0.1 to 0.15. Considering the three disproportionation modes as the characteristic frequencies and assimilating $\omega_{log} = \left(\omega_{Boc}.\omega_{alt-Boc1/2}.\omega_{alt-Boc1/3}\right)^{1/3}$ and a usual screened Coulomb potential μ^*=0.125, a T_c of 22 K is obtained in $Ba_{0.35}K_{0.65}SbO_3$ and a maximal T_c of 30 K is extracted in BKBO for x=0.4-0.5 (**Figure 7.b**). These results are in good agreement with experimental values available in literature with a maximal T_c of 15 K in BKSO (x=0.65) and 32 K in optimally doped BKBO. Furthermore, the global trend of T_c *versus* doping content is well captured by the model, highlighting that the identified disproportionation modes are the determining factor behind the superconducting mechanism of antimonates and bismuthates. It is worth to emphasize that (i) the DFT model may underestimate the doping content needed to reach the SC phase due to band gap underestimation inherent to semi-local DFT functionals and (ii) there are of course uncertainties on T_c associated with the choice of μ^* and the approximation for estimating ω_{log}.

***The ionic nature of antimonates explains their "large" T_c for x>0.65*:** at the same doping content such as x=0.65, the T_c of antimonates is predicted to be higher (22 K) than the T_c of bismuthates (5.7 K), compatible with experimental facts (15 K *vs* 7 K in BKSO and BKBO, respectively, Ref. [19]). Although the B_{oc} mode yields very similar EPC λ for the two compounds, the alternative disproportionation modes alt-$B_{oc1/2}$ and alt-$B_{oc1/3}$ have a larger contribution to the total EPC in antimonates than in bismuthates, resulting in a larger EPC in BKSO (**Figure 7.a**). The larger EPCs originate from a stronger coupling between these structural motions and the electronic structure ($D_{Boc1/2}$=12.5 eV.Å^{-1} in BKSO and 6 eV.Å^{-1} in BKBO, **Figure 6.b**).

***The alt-$B_{oc1/2}$ mode explains the maximal T_c centered at x=0.5 in BKBO*:** Due to its NCT nature, the alt-B_{oc} disproportionation modes are already quenched by the hybridized electronic structure in BKBO. Nevertheless, the alt-$B_{oc1/2}$ mode remains compatible with a half-doped situation and it hence reaches its lowest frequency at x=0.4-0.5. For x>0.5, the mode rapidly hardens upon doping the

compound (**Figure 6.a**). Recalling that λ is inversely proportional to $\omega^2_{\square}$ (**eq.1**), the EPC associated with alt-$B_{oc1/2}$ is maximal for x=0.4-0.5. It results in a plateau for the T_c between x=0.4 and x=0.5 (**Figure 7.b**), in agreement with experiments.

IV. Conclusions

The ionic character and resulting more localized electronic structure of $Ba_{1-x}K_xSbO_3$ explains the high doping content needed to reach the SC phase in the doping phase diagram. At the same time, it produces strongly coupled structural-electronic features sufficient to mediate the formation of Cooper pairs. Nevertheless, the drawback is the resilience of the material to transit to a metallic state with doping and hence to the emergence of a SC state close to soft phonons strongly coupled to the electrons. This situation is reminiscent of the SC nickelates where the starting material is a strong Mott insulator prone to exhibit several CBO upon doping before transiting the SC region for a high doping content [32]. Finally, identifying the relevant, and potentially hidden, electronic and structural instabilities in the doped phase diagram of compounds is a critical aspect for understanding the emergence of superconductivity.

ACKNOWLEDGEMENTS

JV acknowledges access granted to HPC resources of Criann through the projects 2020005 and 2007013 and of Cines through the DARI project A0080911453. This work was supported by the French ANR through the project “SuperNickel”.

REFERENCES

[1] L. N. Cooper, *Bound Electron Pairs in a Degenerate Fermi Gas*, Physical Review **104**, 1189 (1956).

[2] J. Bardeeen, L. N. Cooper, and J. R. Schrieffer, *Theory of Super Conductivity*, Physical Review **108**, 1175 (1957).

[3] B. Keimer, S. A. Kivelson, M. R. Norman, S. Uchida, and J. Zaanen, *From Quantum Matter to High-Temperature Superconductivity in Copper Oxides*, Nature **518**, 179 (2015).

[4] A. Garg, M. Randeria, and N. Trivedi, *Strong Correlations Make High-Temperature Superconductors Robust against Disorder*, Nat Phys **4**, 762 (2008).

[5] H. Li, X. Zhou, S. Parham, T. J. Reber, H. Berger, G. B. Arnold, and D. S. Dessau, *Coherent Organization of Electronic Correlations as a Mechanism to Enhance and Stabilize High-T_c Cuprate Superconductivity*, Nat Commun **9**, 26 (2018).

[6] P. Worm, L. Si, M. Kitatani, R. Arita, J. M. Tomczak, and K. Held, *Correlations Tune the Electronic Structure of Pentalayer Nickelates into the Superconducting Regime*, Phys Rev Mater **6**, L091801 (2022).

[7] M. Kitatani, L. Si, O. Janson, R. Arita, Z. Zhong, and K. Held, *Nickelate Superconductors—a Renaissance of the One-Band Hubbard Model*, npj Quantum Mater **5**, 59 (2020).

[8] C. H. P. Wen et al., *Unveiling the Superconducting Mechanism of $Ba_{0.51}K_{0.49}BiO_3$*, Phys Rev Lett **121**, 117002 (2018).

[9] Z. P. Yin, A. Kutepov, and G. Kotliar, *Correlation-Enhanced Electron-Phonon Coupling: Applications of GW and Screened Hybrid Functional to Bismuthates, Chloronitrides, and Other High-T_c Superconductors*, Phys Rev X **3**, 021011 (2013).

[10] Z. Yuan, P. Zheng, Y. Peng, R. Liu, X. Ma, G. Wang, T. Yu, and Z. Yin, *Correlation-Enhanced Electron-Phonon Coupling and Superconductivity in (Ba, K)SbO_3 Superconductors*, Phys Rev B **105**, 014517 (2022).

[11] Z. Li, G. Antonius, M. Wu, F. H. Da Jornada, and S. G. Louie, *Electron-Phonon Coupling from Ab Initio Linear-Response Theory within the GW Method: Correlation-Enhanced Interactions and Superconductivity in $Ba_{1-x}K_xBiO_3$*, Phys Rev Lett **122**, 186402 (2019).

[12] F. C. Zhang and T. M. Rice, *Effective Hamiltonian for the Superconducting Cu Oxides*, Phys Rev B **37**, 3759 (1988).

[13] L. F. Mattheiss and Haman, *Electronic Structure of $BaPb_{1-x}Bi_xO_3$*, Phys Rev B **28**, 1983 (1983).

[14] A. Khazraie, K. Foyevtsova, I. Elfimov, and G. A. Sawatzky, *Bond versus Charge Disproportionation in the Bismuth Perovskites*, Phys Rev B **98**, 205104 (2018).

[15] M. R. Benam, K. Foyevtsova, A. Khazraie, I. Elfimov, and G. A. Sawatzky, *Bond versus Charge Disproportionation and Nature of the Holes in s-p ABX_3 Perovskites*, Phys Rev B **104**, (2021).

[16] C. Chaillout et al., *Discovery of a Second Family of Bismuth-Oxide-Based Superconductors*, Nature **390**, 148 (1997).

[17] J. G. Bednorz and K. A. Müller, *Possible High Tc Superconductivity in the Ba-La-Cu-O System*, Z. Phys. B - Condensed Matter **64**, 189 (1986).

[18] A. W. Sleight, *Bismuthates: $BaBiO_3$ and Related Superconducting Phases*, Physica C: Superconductivity and Its Applications **514**, 152 (2015).

[19] M. Kim et al., *Superconductivity in (Ba,K)SbO_3*, Nat Mater **21**, 627 (2022).

[20] M. Kim, S. Klenner, G. M. McNally, J. Nuss, A. Yaresko, U. Wedig, R. K. Kremer, R. Pöttgen, and H. Takagi, *Mixed Valence and Superconductivity in Perovskite Antimonates*, Chemistry of Materials **33**, 6787 (2021).

[21] L. F. Mattheiss, E. M. Gyorgy, and D. W. Johnson, *Superconductivity above 20 K in the Ba-K-Bi-O System*, Phys Rev B **37**, 3745 (1988).

[22] A. W. Sleight, J. L. Gillson, and P. E. Bierstedt, *High-Temperature Superconductivity in the $BaPb_{1-x}Bi_xO_3$ System*, Solid State Commun **17**, 27 (1975).

[23] A. Mercy, J. Bieder, J. Íñiguez, and P. Ghosez, *Structurally Triggered Metal-Insulator Transition in Rare-Earth Nickelates*, Nat Commun **8**, 1 (2017).

[24] J. Varignon, *Origin of Superconductivity in Hole Doped $SrBiO_3$ Bismuth Oxide Perovskite from Parameter-Free First-Principles Simulations*, npj Comput Mater **9**, 30 (2023).

[25] J. W. Furness, A. D. Kaplan, J. Ning, J. P. Perdew, and J. Sun, *Accurate and Numerically Efficient R2SCAN Meta-Generalized Gradient Approximation*, Journal of Physical Chemistry Letters **11**, 8208 (2020).

[26] G. Kresse and J. Furthmüller, *Efficiency of Ab-Initio Total Energy Calculations for Metals and Semiconductors Using a Plane-Wave Basis Set*, Comput Mater Sci **6**, 15 (1996).

[27] G. Kresse and Hafner J., *Ab. Initio Molecular Dynamics for Liquid Metals*, Phys Rev B **47**, 558(R) (1993).

[28] P. E. Blöchl, *Projector Augmented-Wave Method*, Phys Rev B **50**, 17953 (1994).

[29] A. Zunger, S.-H. Wei, L. G. Ferreira, and J. E. Bernard, *Special Quasirandom Structures*, Phys. Rev. Lett. **65**, 353 (1990).

[30] L. Iglesias, M. Bibes, and J. Varignon, *First-Principles Study of Electron and Hole Doping Effects in Perovskite Nickelates*, Phys Rev B **104**, 035123 (2021).

[31] *A Supplementary Material Can Be Found at Xxxx*.

[32] A. A. Carrasco-Alvarez, S. Petit, L. Iglesias, M. Bibes, W. Prellier, and J. Varignon, *Electron-Phonon Mediated Superconductivity in $R_6Ni_5O_{12}$ Nickel Oxides*, ArXiv.2311.13674 (2023).

[33] P. B. Allen and R. C. Dynes, *Transition Temperature of d-f-Band Superconductors*, Phys Rev B **12**, 905 (1975).

[34] G. Pizzi et al., *Wannier90 as a Community Code: New Features and Applications*, Journal of Physics Condensed Matter **32**, 165902 (2020).

[35] A. A. Mostofi, J. R. Yates, Y.-S. Lee, I. Souza, D. Vanderbilt, and N. Marzari, *Wannier90: A Tool for Obtaining Maximally-Localised Wannier Functions*, Comput Phys Commun **178**, 685 (2008).

[36] A. A. Mostofi, J. R. Yates, G. Pizzi, Y. S. Lee, I. Souza, D. Vanderbilt, and N. Marzari, *An Updated Version of Wannier90: A Tool for Obtaining Maximally-Localised Wannier Functions*, Comput Phys Commun **185**, 2309 (2014).

[37] V. Popescu and A. Zunger, *Extracting e versus k - Effective Band Structure from Supercell Calculations on Alloys and Impurities*, Phys Rev B **85**, 085201 (2012).

[38] H. T. Stokes and D. M. Hatch, *FINDSYM: Program for Identifying the Space-Group Symmetry of a Crystal*, J Appl Crystallogr **38**, 237 (2005).

[39] D. Orobengoa, C. Capillas, M. I. Aroyo, and J. M. Perez-Mato, *AMPLIMODES: Symmetry-Mode Analysis on the Bilbao Crystallographic Server*, J Appl Crystallogr **42**, 820 (2009).

[40] *ISOTROPY Software Suite, Iso.Byu.Edu*, https://iso.byu.edu/iso/isodistort_version5.6.1/isodistort.php.

[41] B. G. Jang, M. Kim, S. H. Lee, W. Yang, S. H. Jhi, and Y. W. Son, *Intersite Coulomb Interactions in Charge-Ordered Systems*, Phys Rev Lett **130**, (2023).

[42] M. Kim, S. Klenner, G. M. McNally, J. Nuss, A. Yaresko, U. Wedig, R. K. Kremer, R. Pöttgen, and H. Takagi, *Mixed Valence and Superconductivity in Perovskite Antimonates*, Chemistry of Materials **33**, 6787 (2021).

[43] J. Varignon, M. Bibes, and A. Zunger, *Origins Vs. Fingerprints of the Jahn-Teller Effect in d-Electron ABX_3 Perovskites*, Phys Rev Res **1**, 033131 (2019).

[44] J. Varignon, M. Bibes, and A. Zunger, *Origin of Band Gaps in 3d Perovskite Oxides*, Nat Commun **10**, 1658 (2019).

[45] J. Varignon, O. I. Malyi, and A. Zunger, *Dependence of Band Gaps in d -Electron Perovskite Oxides on Magnetism*, Phys Rev B **105**, 165111 (2022).

[46] G. A. Baraff, E. O. Kane, and M. Schlüter, *Theory of the Silicon Vacancy: An Anderson Negative-U System*, Phys Rev B **21**, 5662 (1980).

[47] Y. Nagata, A. Mishiro, T. Uchida, M. Ohtsuka, and H. Samata, *Normal-State Transport Properties of $Ba_{1-x}K_xBiO_3$ Crystals*, Journal of Physics and Chemistry of Solids **60**, 1933 (1999).

[48] D. C. Kim, A. N. Baranov, J. S. Kim, H. R. Kang, B. J. Kim, Y. C. Kim, J. S. Pshirkov, E. V Antipov, and Y. W. Park, *Superconductivity of $Ba_{1-x}K_xBiO_3$ ($0.35 < x < 1$) Synthesized by the High Pressure and High Temperature Technique*, Journal Of Superconductivity: Incorporating Novel Magnetism **15**, 331 (2002).